

Article

Influence of Critical Wall Roughness on the Performance of Double-Channel Sewage Pump

Xiaoke He ¹, Yingchong Zhang ², Chuan Wang ^{3,*} , Congcong Zhang ³, Li Cheng ^{3,*}, Kun Chen ⁴ and Bo Hu ⁵ 

¹ School of Electric Power, North China University of Water Resources and Electric Power, Zhengzhou 450045, China; hexiaoke@ncwu.edu.cn

² National Research Center of Pumps, Jiangsu University, Zhenjiang 212013, China; zhangyingchong1994@163.com

³ College of Hydraulic Science and Engineering, Yangzhou University, Yangzhou 225009, China; Conniezcc@163.com

⁴ Ningbo Jushen Pumps Industry Co., Ltd., Ningbo 315100, China; skyckun2009@163.com

⁵ Deputy Energy & Power Engineering, Tsinghua University, Beijing 100084, China; hubo@mail.tsinghua.edu.cn

* Correspondence: wangchuan@ujs.edu.cn (C.W.); chengli@yzu.edu.cn (L.C.)

Received: 22 November 2019; Accepted: 13 January 2020; Published: 17 January 2020



Abstract: The numerical method on a double-channel sewage pump was studied, while the corresponding experimental result was also provided. On this basis, the influence of wall roughness on the pump performance was deeply studied. The results showed that there was a critical value of wall roughness. When the wall roughness was less than the critical value, it had a great influence on the pump performance, including the head, efficiency, and shaft power. As the wall roughness increased, the head and efficiency were continuously reduced, while the shaft power was continuously increased. Otherwise, the opposite was true. The effect of wall roughness on the head and hydraulic loss power was much smaller than that on the efficiency and disk friction loss power, respectively. With the increase of wall roughness, mechanical efficiency and hydraulic efficiency reduced constantly, leading to the decrement of the total efficiency. With the increase of flow rate, the effect of wall roughness on the head and efficiency gradually increased, while the influence on the leakage continuously reduced. The influence of the flow-through component roughness on the pump performance was interactive.

Keywords: double-channel sewage pump; critical wall roughness; numerical calculation; external characteristics

1. Introduction

Pumps are classified as general machinery with varied applications [1–5]. Sewage pump, as important equipment in the sewage treatment project, is widely used in chemical, municipal, and other industries. It is mainly used to transport production and domestic sewage containing a large amount of solid particles or fibrous solid substances. The double-channel sewage pump has the characteristics of compact structure, high efficiency, and good anti-winding and anti-clogging performance, while it has a wide application range, which has been studied by a large number of scholars [6–10].

It is well known that pumps have huge energy consumption, and wall roughness has an important effect on pump efficiency [11–16]. In the process of using the double-channel sewage pump, the abrasion of the wall surface caused by the impurities in the transport medium and the damage of the blade surface caused by erosion will cause the change of the wall roughness, and roughness Ra is one of the important factors affecting the performance of the pump.

2. Literature Overview

In the past years, many scholars studied the effect of wall roughness on the flow in pipes, fans, compressors, microchannels. In order to study the effect of wall roughness in turbulent pipe flow, Hemeida [17] developed an equation for estimating the thickness of the laminar sublayer in turbulent pipe flow of pseudoplastic fluids and found that the turbulent pipe flow could be divided into two regions: smooth wall and rough wall turbulence. The roughness Reynolds number was used to determine the smooth wall turbulence and rough wall turbulence regions. Kandlikar [18] studied the roughness effects at microscale—reassessing Nikuradse’s experiments on liquid flow in rough tubes, and found that Nikuradse’s work was revisited in light of the recent experimental work on roughness effects in microscale flow geometries. Li et al. [19] studied the influence of the internal surface roughness of the nozzle on cavitation erosion characteristics of submerged cavitation jets from the aspects of erosion intensity and erosion efficiency; it could be concluded that excessive smooth surface was not conducive to the formation of cavitation bubbles, leading to an attenuated intensity of cavitation erosion, while excessive rough surface caused much energy dissipation and led to divergent jets, resulting in a significant reduction of erosion intensity. According to the experimental results, there existed an optimum inner surface roughness value to achieve the strongest aggressive cavitation erosion capability for submerged cavitating jets. Tang et al. [20] analyzed the existing experimental data in the literature on the friction factor in microchannels. The friction factors in stainless steel tubes were much higher than the theoretical predictions for tubes of conventional size. This discrepancy resulted from the large relative surface roughness in the stainless steel tubes. From the literature review and the present test data, it is suggested that for gaseous flow in microchannels, with relative surface roughness less than 1%, the conventional laminar prediction should still be applied. Gamrat et al. [21] used three different approaches in the present study to predict the influence of roughness on laminar flow in microchannels. The numerical simulations, the rough layer model, and the experiments agreed to show that the Poiseuille number Po increased with the relative roughness and was independent of Re in the laminar regime ($Re < 2000$). The increase in Po observed during the experiments was predicted well both by the three-dimensional simulations and the rough layer model. Li et al. [22] studied the effect of the roughness of the compressor blade on the performance based on the equivalent Reynolds number correction principle and found that when the surface roughness increased, the main characteristic parameters of the compressor were reduced to varying degrees, making the compressor overall performance degraded. Li et al. [23] discussed the formula for calculating friction loss of fluid flow in similar fan ducts. The calculation formulas between the model and the physical flow efficiency under different relative surface roughness of the flow channel were introduced. Li et al. [24] studied the effect of surface roughness on the micro-gap leakage of oil-free lubrication scroll compressors and found that under the condition of the same micro-gap size and inlet pressure, a larger rough element height and distribution density could effectively increase the leakage. The flow resistance of the gas reduced the leakage flow rate, thereby reducing the amount of leakage. Gao [25] used low-speed compressor plane cascade experiments to study the effect of different roughness positions on cascade performance. It was found that cascade performance was more sensitive to leading-edge roughness and suction front roughness. In terms of roughness, the total pressure loss value was reduced by 23.1% compared to the smooth blade. Han et al. [26] used numerical methods to study the influence of blade surface roughness on the internal flow field and characteristic parameters of the compressor under the compressor-level environment and found that the blade roughness had a significant effect on the main performance parameters of the compressor; with the blade roughness with the increase of the compressor, the performance degradation of the compressor stage was intensified, and the energy loss of the internal airflow was increased, especially the energy loss of the airflow near the middle and upper part of the leading edge of the impeller was severe, and the temperature of the blade end wall was increased.

With the rapid development of computer technology, numerical simulation is increasingly widely used in the fluid flow [27–33]. Guelich et al. [34] studied the effect of wall roughness on the efficiency

of centrifugal pumps. It was found that the effect of wall roughness in the volute was stronger than the roughness inside the impeller. The magnitude of hydraulic loss depended on the wall roughness, turbulent flow near the wall, and actual velocity distribution in the flow channel. Zhu et al. [35] simulated the influence of wall roughness of flow parts, including impeller, diffuser, pump cavity, and hub, on the performance of the axial flow pump and found that reducing the roughness of the flow surface could effectively improve the head and efficiency. The efficiency of the axial flow pump was more sensitive to changes in the roughness of the blade surface. Yamazaki et al. [36] studied the effect of wall roughness on the performance of jet pumps. It was found that the wall roughness near the throat inlet had the greatest influence on the efficiency of the jet pump. The optimum efficiency decreased linearly with increasing wall roughness. Aldas et al. [37] used CFD numerical calculation to determine the effect of pump absolute roughness and relative roughness on pump efficiency. It was found that under certain absolute roughness, the efficiency was significantly improved until a certain degree. Feng et al. [38] found that under the optimal condition, compared with no roughness, when the roughness was 3.2 μm , 6.3 μm , and 12.5 μm , the head decreased by 0.3 m, 0.5 m, and 0.7 m, while the efficiency decreased by 4.7%, 5.7%, and 6.8%. Pan et al. [39] obtained the performance difference of the axial flow pump under the influence of different rough wall through simulation calculation. It was found that under the influence of wall roughness, the pump device showed a decrease in the head and the efficiency, and the efficiency decreased most. Deshmukh et al. [40] analyzed the turbulent flow energy and eddy viscosity characteristics of electric submersible pumps with different roughness, and the influence of wall disturbance on the pressure distribution and velocity field. It was found that the roughness effect of the high viscosity oil was the most significant relative to water. Under non-design conditions, the Reynolds number affects the overall roughness effect. Gu et al. [41] used the experimental design method, based on the numerical simulation technology to test the design and simulation of the head, shaft power, and efficiency of the axial flow pump. It was found that the impeller wall roughness had the greatest influence on the hydraulic performance, the influence coefficient on the head was -0.265 , while efficiency was -0.283 , and the shaft power was 0.099 . Lim [42] studied the effect of wall roughness of the double-suction centrifugal pump components on performance. It was found that the impeller roughness had the greatest influence on the performance of the double suction centrifugal pump, while the suction chamber had the least impact. Pump performance had a strong correlation with the wall roughness of the impeller cover. To sum up, many scholars only study the effect of wall roughness on pump efficiency, but there are few manuscripts on critical wall roughness.

In this paper, numerical and experimental studies were made in a double-channel sewage pump. The influence of critical wall roughness on the performance of the pump was analyzed, which had practical guiding significance for the production, maintenance, and daily management of the double-channel sewage pump.

3. Numerical Calculation

3.1. Calculation Model

The design parameters of the double-channel sewage pump were as follows: rated flow $Q_d = 12 \text{ m}^3/\text{h}$, rated head $H = 13 \text{ m}$, impeller speed $n = 2800 \text{ r/min}$, impeller blade number $Z = 2$, specific speed $n_s = 3.65nQ^{0.5}/H^{0.75} = 86$. Impeller and volute were the core components of the pump. Due to the requirement of non-blocking performance, the impeller of the sewage pump adopted a curved pipe shape, and the volute section adopted a rectangular section, as shown in Figure 1. The geometric parameters of the impeller and volute were calculated by the velocity coefficient method, as shown in Table 1. The calculation model was the basis of numerical calculation, and the integrity of the model had a significant impact on the accuracy of the calculation results. If only the impeller and volute were considered, the disk friction loss and volume leakage loss were neglected. Therefore, to study the influence of wall roughness on the performance of the pump more accurately, the calculation model of

the pump included the ring clearance, the impeller, the pump cavity, the volute, the inlet, and outlet sections whose length were 5 times and 10 times of impeller outlet diameter, as shown in Figure 2.

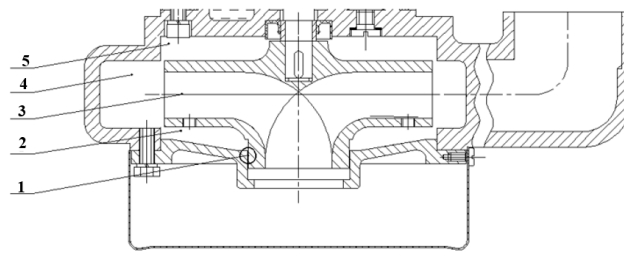


Figure 1. Schematic diagram of the double-channel sewage pump. 1. Ring clearance; 2. Front pump cavity; 3. Impeller; 4. Volute; 5. Rear pump cavity.

Table 1. Basic geometric parameters of the pump.

Geometric Parameters	Numerical Value	Geometric Parameters	Numerical Value
Impeller inlet diameter D_j (mm)	30	Blade outlet angle β_2 ($^\circ$)	22.5
Impeller outlet diameter D_2 (mm)	107	Volute base diameter D_3 (mm)	124
Impeller outlet width b_2 (mm)	20	Volute inlet width b_3 (mm)	30
Blade inlet angle β_1 ($^\circ$)	68	Volute outlet diameter D_d (mm)	44

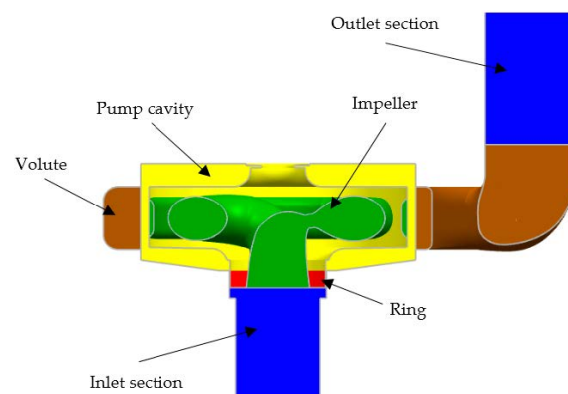


Figure 2. Calculation model of the double-channel sewage pump (most of the inlet and outlet sections are hidden).

3.2. Grid Independence

Compared with the common centrifugal pump impeller, the impeller of the double-channel sewage pump had the characteristics of severe distortion, large wrap angle, and special profile. Therefore, in the ICEM (Integrated Computer Engineering and Manufacturing), the hexahedral structured grid was generated for the total calculation domain of the double-channel sewage pump, as shown in Figure 3. In order to determine the appropriate number of grids, five grid sizes (G values) were selected for the grid-independent analysis under the same settings, as shown in Figure 4. It could be seen that the influence of the grid size G on the pump performance was within 2%. When the grid size was large, that is, the grid number was small, the efficiency η and head H were relatively high. When $G \leq 1.5$ mm, the efficiency and head were basically stable. Considering the coordination of calculation accuracy and time, $G = 1.5$ mm was selected for meshing, as shown in Figure 3. Moreover, the grid quality of the calculation model can be seen in Table 2. The total grid quality was more than 0.37, which could meet the requirement of the numerical calculation.

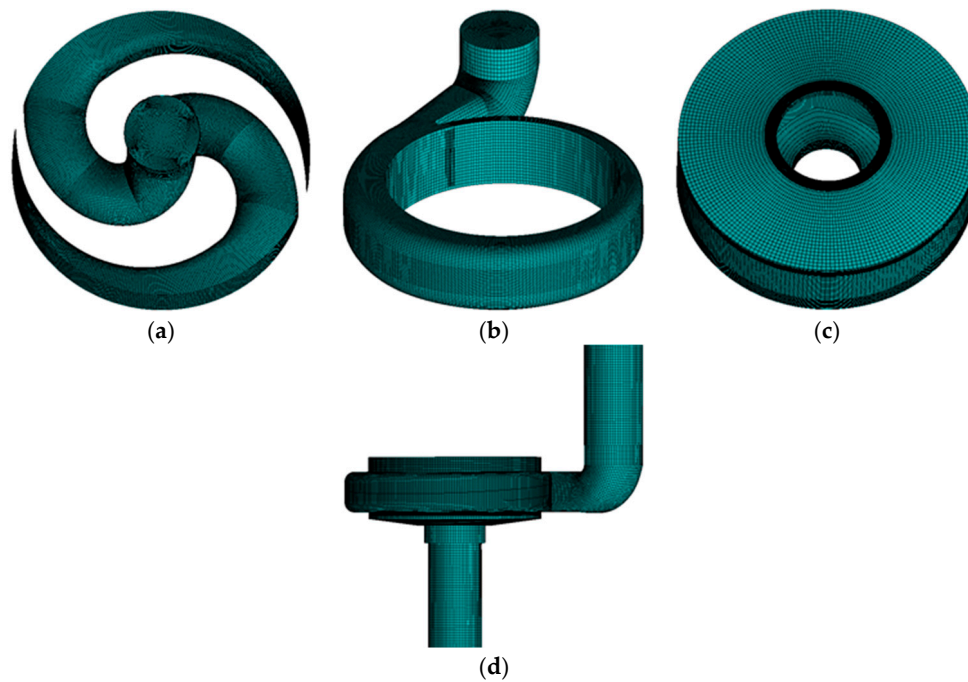


Figure 3. Structure meshing. (a) Impeller, (b) Volute, (c) Pump cavity, (d) Overall domain.

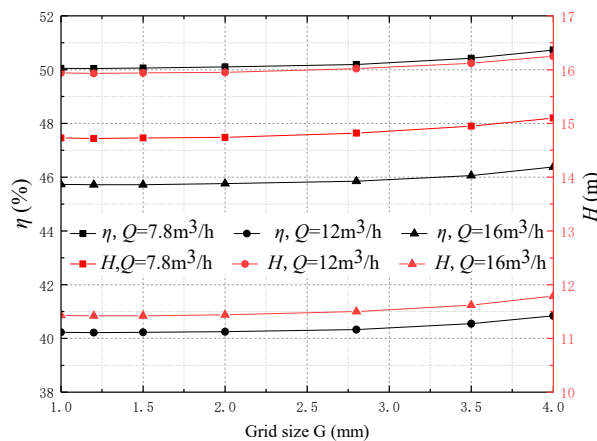


Figure 4. Grid independence analysis.

Table 2. Grid quality.

Parts	Grid Number	Node Number	Impeller	Volute	Pump Cavity	Inlet Section	Outlet Section
Grid quality	4,839,030	4,289,372	0.37	0.43	0.54	0.65	0.63

3.3. Turbulent Model

Turbulence models for pumps in ANSYS CFX (Computational Fluid X) include standard $k-\epsilon$ (k and ϵ represent the pulsating kinetic energy of the turbulent flow and its dissipation rate respectively), RNG (Renormalization-group) $k-\epsilon$, SST (shear stress transport), $k-\omega$ (ω represents another kind of dissipation rate) and others. The calculation results of different turbulence models were quite different and needed to be selected according to the actual situation. Therefore, the numerical calculations with different turbulence modes under the rated flow condition were carried out and compared with the experimental results, as shown in Table 3. It was found that the numerical results of the standard $k-\epsilon$ turbulence model agreed well with the experimental results. Therefore, the standard $k-\epsilon$ turbulence model was selected.

Table 3. Experimental and numerical results with different turbulent models under the rated flow condition.

Turbulent Models	Efficiency η (%)	Head H (m)
$k-\varepsilon$	50.06	14.73
RNG $k-\varepsilon$	51.12	14.77
SST	62.89	14.92
$k-\omega$	62.97	14.93
Experimental value	48.09	14.34

3.4. Boundary Setting

The impeller and the shroud in the pump cavity were based on the rotating reference frame, whereas the other sub-domains were based on the stationary reference frame throughout the entire calculation domains. The interfaces between the impeller and its adjacent sub-domains were set to “frozen rotor” mode, and the other interfaces were set to “general connection” mode. Moreover, the non-slip walls were selected as the wall boundaries. The open inlet and mass outflow were selected as the inlet and outlet boundaries.

3.5. Equivalent Sand Model

In actual production, the wall roughness has peaks and valleys, and its shape and size are different. The arithmetic average deviation of the profile (R_a) and unevenness ten-point height (R_z) are the two typical parameters that can illustrate the value of the surface roughness. For simplicity, R_a , the arithmetic average deviation of the profile, was selected in the manuscript.

The wall function method used by CFX is an extension of the method proposed by Launder and Spalding. In the logarithmic regular region, the near-wall tangential velocity of the fluid was logarithmically related to the wall shear stress, and the empirical formula was used to connect the near-wall boundary conditions of the average flow and the turbulent transport equation. The logarithmic relationship of the near-wall velocity was as follows [43]:

$$u^+ = \frac{U_t}{u_\tau} = \frac{1}{\kappa} \ln(y^+) + C \quad (1)$$

$$y^+ = \frac{\rho \Delta y u_\tau}{\mu} \quad (2)$$

$$u_\tau = \sqrt{\frac{\tau_w}{\rho}} \quad (3)$$

where u^+ is the near-wall velocity (in m/s), u_τ is the friction velocity (in m/s), U_t is the tangential velocity at a distance from the wall surface Δy (in m/s), y^+ is the dimensionless distance from the wall, τ_w is the wall shear stress (in N), κ is the Von Karman constant, C is a constant associated with wall roughness.

Surface roughness increased the generation of turbulence near the wall, which, in turn, led to a significant increase in wall shear stress, destroying the viscous sub-layer in the turbulent flow. The logarithmic velocity profile near the wall moved down:

$$u^+ = \frac{1}{\kappa} \ln(y^+) + B - \Delta B \quad (4)$$

where B take 5.2, offset ΔB is a function of dimensionless roughness h^+ ($h^+ = hu_\tau/\nu$); ν is kinematic viscosity (in m^2/s).

For grit roughness, the offset ΔB could be expressed in the following form using the dimensionless sand roughness h_s^+ :

$$\Delta B = \frac{1}{\kappa} \ln(1 + 0.3h_s^+) \quad (5)$$

There are usually two methods for measuring roughness in production and life. One is to measure the roughness of the surface of an object by means of a roughness measuring instrument [44,45]. The second is to compare the roughness samples [46], compare the surface roughness of the object with the standard surface roughness samples, and estimate the size of the object surface roughness. The contour arithmetic mean deviation R_a was used as a measurement parameter of roughness, which was defined as follows:

$$R_a = \frac{1}{N} \sum_{i=1}^n |z_i - z| \quad (6)$$

In actual production, the roughness has peaks and valleys, the shape and size are different. In CFX, the equivalent sand roughness k_s was described [47,48], that is, a tightly arranged ball of equal diameter h_s is placed on the smooth plane. Simulating the undulating wall surface, the equivalent sand grain roughness only affected the fluid in the upper half of the ball, as shown in Figure 5. Therefore, the effect of the same surface roughness and the equivalent sand roughness on the fluid was quite different.

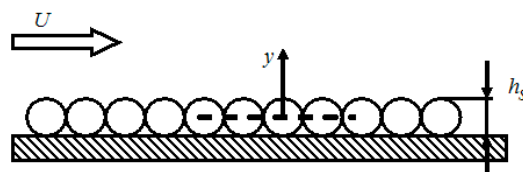


Figure 5. Schematic diagram of CFX equivalent sand model.

Colebrook et al. [49] used the equivalent sand model to experimentally study the gas in rough pipes and found the relationship between “smooth” law and “rough” law. The sand-grain roughness values required for use with the moody chart were not derived from any direct measure of roughness using modern surface characterization equipment, such as an optical profilometer. Using direct measurements of surface roughness in fluid flow calculations might, therefore, result in significant error.

For the equivalent sand model, it could be obtained from formula (6):

$$R_a = \frac{1}{h_s} \sum_{i=1}^{h_s} |y_i - y| \quad (7)$$

When the number of points tended to infinity, formula (7) became the integral formula:

$$R_a = \frac{1}{h_s} \int_{x=0}^{h_s} |y - \bar{y}| dx \quad (8)$$

and

$$\bar{y} = \frac{\pi h_s}{8} \quad (9)$$

Taking Equations (8) and (9) into Equation (7) gave:

$$h_s = 11.03R_a \quad (10)$$

Equation (8) showed that if a roughness meter was used to measure the roughness R_a of a surface composed of a sphere layer with a diameter of h_s , the final value of the measured roughness R_a was an order of magnitude smaller than a suitable sand grain roughness.

Adams et al. [50] proposed an algorithm to convert the measured surface roughness parameters into equivalent sand grain roughness and used this algorithm to convert the surface roughness into equivalent sand grain roughness so that the experimental results and numerical calculation of fluid flow had better consistency. Adams et al. obtained through deduction and experiment:

$$k_s = [(1.2 \pm 0.1)/0.204]R_a = (5.392 \sim 6.372)R_a \quad (11)$$

Combining the research of Deshmukh [51] and so on, the conversion coefficient of the equivalent roughness k_s and the average deviation R_a of the contour arithmetic was selected as:

$$k_s = 5.863R_a \quad (12)$$

The conversion between the wall roughness R_a and the equivalent sand roughness k_s was utilized in CFX, and as shown in Table 4, the numerical calculation regarding the roughness of the double-channel sewage pump was performed.

Table 4. Conversion between the wall roughness R_a and the equivalent sand roughness k_s .

Wall Roughness R_a (μm)	Equivalent Sand Roughness k_s (μm)
0	0
20	117.26
40	234.52
50	293.15
60	351.78
80	469.04
100	586.30

4. Influence of Wall Roughness on the Pump Performance

4.1. Influence of Wall Roughness on the Pump Performance

Six wall roughness of 0 μm , 20 μm , 40 μm , 50 μm , 60 μm , 80 μm , and 100 μm were selected for the numerical calculation of double-channel sewage pump. From Figure 6 and Table 5, it could be seen that there was a critical wall roughness ($R_a = 50 \mu\text{m}$) for the influence of roughness on the performance of the pump. When $0 \mu\text{m} \leq R_a \leq 50 \mu\text{m}$, with the increase of R_a , the head H and efficiency η gradually decreased, and the decreasing rate gradually reduced, while the shaft power P gradually increased, and the increasing rate gradually decreased. When $50 \mu\text{m} \leq R_a \leq 100 \mu\text{m}$, with the increase of R_a , H and η gradually increased, and the increasing rate gradually decreased, while P decreased gradually, and the decreasing rate gradually reduced. When R_a increased from 0 μm to 50 μm , the value of P increased by 43.39%, and the reductions of H and η were 33.18% and 4.12%, respectively. It showed that when the wall roughness was less than the critical wall roughness, the wall roughness had a great influence on the performance of the pump, and the influence on the shaft power and efficiency was much greater than that on the head. When the wall roughness was larger than the critical wall roughness, the wall roughness had little effect on the performance of the pump.

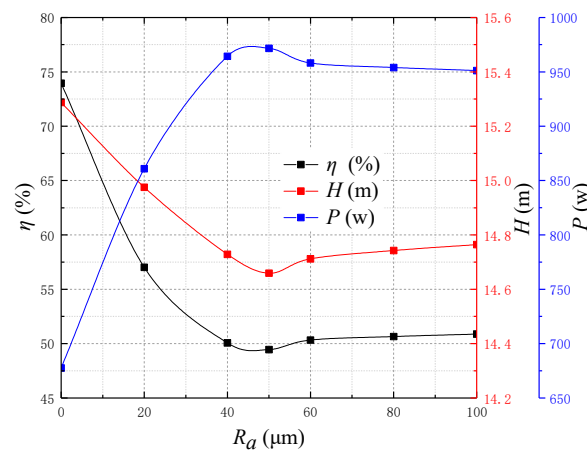


Figure 6. Pump performance of the pump with different wall roughness under the rated flow condition.

Table 5. Pump performance with different roughness under the rated flow condition.

Roughness R_a (μm)	0	20	40	50	60	80	100
Efficiency η (%)	73.95	57.02	50.06	49.45	50.33	50.65	50.87
Head H (m)	15.29	14.98	14.73	14.66	14.71	14.74	14.76
Shaft power P (w)	677.54	860.83	964.28	971.55	958.14	953.97	951.17

4.2. Influence of Wall Roughness on the Internal Flow of the Pump

The influence of wall roughness on the internal flow of the pump could be expressed by the turbulent energy. Estimating the turbulent kinetic energy using turbulence intensity, the formula was as follows:

$$k = \frac{3}{2}(ul)^2 \quad (13)$$

$$l = 0.16 \times R_e^{-1/8} \quad (14)$$

where u is the average velocity (in m/s), l is the turbulence intensity, and R_e is the Reynolds number. Figure 7 shows the turbulence energy distribution in the middle section of the pump with different wall roughness under the rated flow condition ($Q = 12 \text{ m}^3/\text{h}$). It could be seen that due to the influence of the impeller's rotation, the turbulent energy was gradually reduced from the shroud edge to the shroud center. There was the largest turbulent energy at the clearance ring, so the domain of the clearance ring could not be ignored in the numerical calculation. As the wall roughness increased, the turbulent flow energy k gradually increased, and the increasing rate gradually reduced.

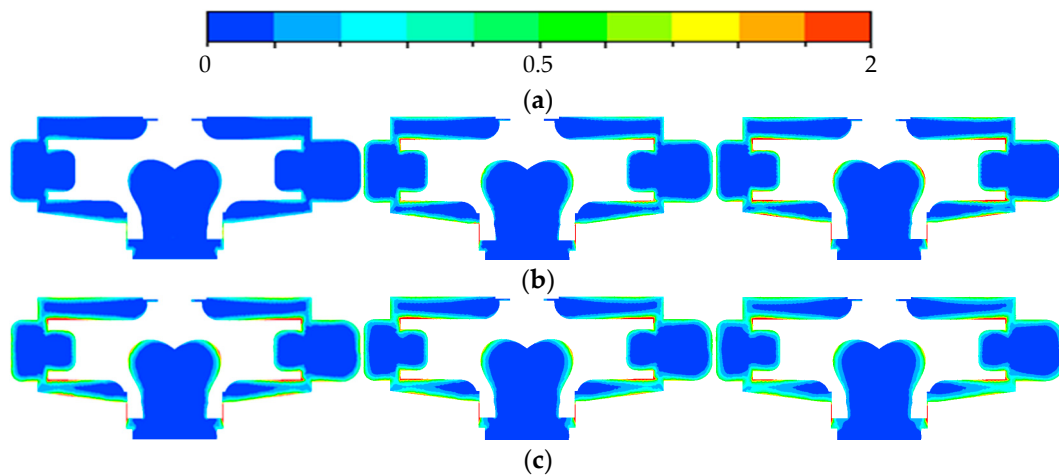


Figure 7. Turbulence energy distribution in the middle section of the pump with different wall roughness under the rated flow condition. (a) Turbulence kinetic energy (m^2/s^2), (b) $R_a = 0 \mu\text{m}$, $k = 0.096 \text{ m}^2/\text{s}^2$; $R_a = 20 \mu\text{m}$, $k = 0.217 \text{ m}^2/\text{s}^2$; $R_a = 40 \mu\text{m}$, $k = 0.278 \text{ m}^2/\text{s}^2$, (c) $R_a = 60 \mu\text{m}$, $k = 0.307 \text{ m}^2/\text{s}^2$; $R_a = 80 \mu\text{m}$, $k = 0.327 \text{ m}^2/\text{s}^2$; $R_a = 100 \mu\text{m}$, $k = 0.346 \text{ m}^2/\text{s}^2$.

The variation of the hydraulic loss distribution inside the impeller was related to the pressure distribution. Figure 8 shows the pressure distribution in the middle section of the pump with different wall roughness under the rated flow condition. It could be seen that the pressure inside the impeller was center-symmetric. As the wall roughness increased, the pressure inside the impeller gradually decreased, mainly at the edge of the impeller, and the decreasing rate gradually reduced.

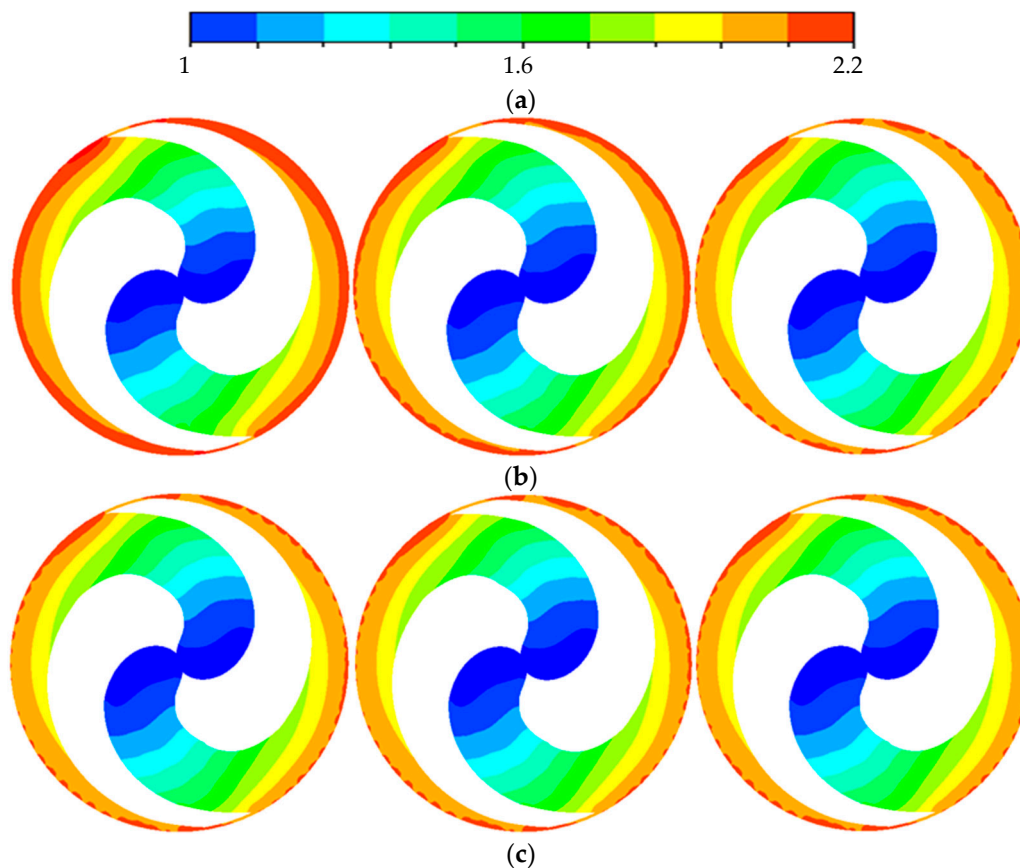


Figure 8. Pressure distribution in the middle section of the pump with different wall roughness under the rated flow condition. (a) Static pressure (10^5 pa), (b) $R_a = 0$ μm , Pressure = 113,484 Pa; $R_a = 20$ μm , Pressure = 96,037 Pa; $R_a = 40$ μm , Pressure = 95,091 Pa, (c) $R_a = 60$ μm , Pressure = 94,068 Pa; $R_a = 80$ μm , Pressure = 93,088 Pa; $R_a = 100$ μm , Pressure = 94,248 Pa.

4.3. Influence of Wall Roughness on the Components of the Efficiency and Shaft Power

In order to study why the influence of wall roughness on the performance of the pump is so obvious, this paper further subdivided the external characteristic of the pump. The components of its shaft power and efficiency are shown in Table 6. Without considering the mechanical loss at the bearing shaft seal, the formulae were as follows:

$$\eta = \frac{\rho g Q H}{P} \quad (15)$$

$$P = P_m + P_h \quad (16)$$

$$P_m = M \omega \quad (17)$$

The three sub-efficiencies of the pump were obtained from the following formulae:

$$\eta_m = 1 - \frac{P_m}{P} \quad (18)$$

$$\eta_v = \frac{Q}{Q + q} \quad (19)$$

$$\eta_h = \frac{\eta}{\eta_m \eta_v} \quad (20)$$

where P is the shaft power (in W), P_m is the disk friction loss power (in W), P_h is the hydraulic power (in W), q is the average ring leakage (in m^3/h), η_m is the mechanical efficiency, η_v is the volumetric efficiency, and η_h is the hydraulic efficiency.

Table 6. Pump's performance with different wall roughness under the rated flow condition.

R_a (μm)	P_m (W)	P_h (W)	P (W)	Q (m^3/h)	q (m^3/h)	η_m (%)	η_v (%)	η_h (%)	η (%)
0	46.53	631.01	677.54	12	0.82	93.13	93.59	84.84	73.95
20	155.40	705.43	860.83	12	0.99	81.95	92.37	75.33	57.02
40	216.01	748.27	964.28	12	1.03	77.60	92.10	70.05	50.06
50	224.65	746.90	971.55	12	1.06	76.88	91.90	70.00	49.45
60	217.53	740.60	958.14	12	1.07	77.30	91.87	70.87	50.33
80	212.25	741.73	953.97	12	1.07	77.75	91.83	70.94	50.65
100	208.80	742.37	951.17	12	1.08	78.05	91.77	71.03	50.87

Figure 9 illustrates the three kinds of power P_m , P_h , and P with different wall roughness R_a under the rated flow conditions ($Q = 12 \text{ m}^3/\text{h}$). When $0 \mu\text{m} \leq R_a \leq 50 \mu\text{m}$, as R_a increased, P_m , P_h , and P increased together, but the increasing rate gradually reduced; when $50 \mu\text{m} \leq R_a$, as R_a increased, P_m , P_h and P decreased slightly. When R_a changed from $0 \mu\text{m}$ to $50 \mu\text{m}$, P_m and P_h increased to 382.81% and 18.37%, respectively. When R_a changed from $50 \mu\text{m}$ to $100 \mu\text{m}$, P_m and P_h increased to 7.06% and 0.61%, respectively, indicating that when the wall roughness did not reach the critical wall roughness, the influence of the wall roughness was relatively large. The effect of the wall roughness on P_h was much smaller than that on P_m .

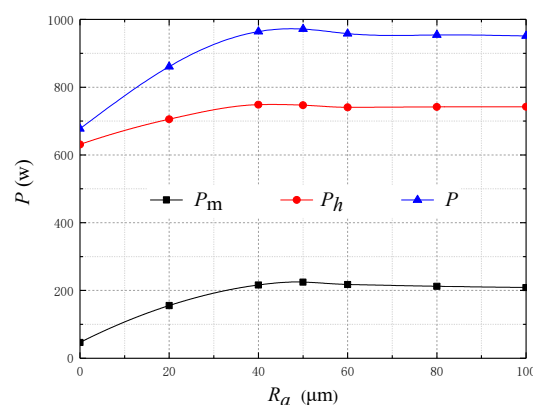


Figure 9. Three kinds of power of the pump with different wall roughness under the rated flow condition.

Figure 10 shows the pump mechanical efficiency η_m , hydraulic efficiency η_h , and volumetric efficiency η_v with different roughness R_a under the rated flow condition. It could be seen from Table 5 that as R_a increased, η_v gradually decreased, but the decreasing rate gradually reduced. When R_a did not reach the critical wall roughness ($R_a = 50 \mu\text{m}$), with the increase of R_a , η_m and η_h gradually decreased, and the decreasing rate gradually reduced. When R_a exceeded the critical wall roughness, as R_a increased, η_m and η_h gradually increased, but the increasing rate gradually reduced. When R_a changed from $0 \mu\text{m}$ to $50 \mu\text{m}$, η_m , η_h , and η_v reduced by 16.25%, 14.84%, and 1.69%, respectively. When R_a increased from $50 \mu\text{m}$ to $100 \mu\text{m}$, η_m and η_h increased by 1.17% and 1.03%, and η_v reduced by 0.13%. It showed that when the wall roughness did not reach the critical wall roughness, the effect of wall roughness on the efficiency was large; when the roughness exceeded the critical roughness, the effect of wall roughness on the efficiency was small. With the increase of wall roughness, mechanical efficiency and hydraulic efficiency reduced constantly, leading to the decrement of the total efficiency.

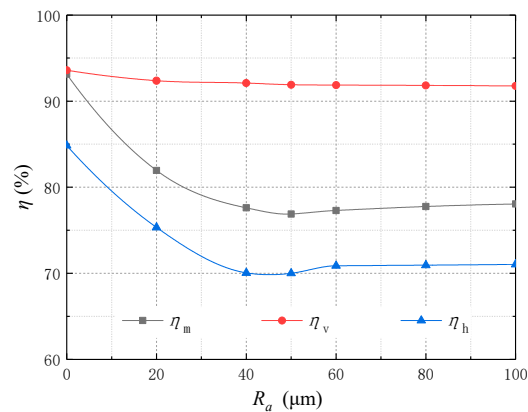


Figure 10. Three kinds of power of the pump with different wall roughness under the rated flow condition.

4.4. Influence of Wall Roughness on the Pump Performance Under Five Flow Conditions

Because of complicated use situations, the pump's operating conditions of the pump were constantly changing. The above research was mainly to study the influence of wall roughness of the pump under the rated flow condition. Therefore, the influence of different wall roughness under five flow conditions ($Q = 7.8, 10, 12, 14,$ and $16 \text{ m}^3/\text{h}$) was numerically calculated, as shown in Table 7.

Table 7. Pump's performance with five flow conditions and wall roughness.

Q (m^3/h)	R_a (μm)	H (m)	P_m (W)	P_h (W)	q (m^3/h)	η_m (%)	η_v (%)	η_h (%)	η (%)
7.8	0	16.13	43.50	505.41	0.84	92.08	90.33	75.04	62.41
10	0	15.90	43.95	568.54	0.83	92.82	92.32	82.44	70.65
12	0	15.29	46.53	631.01	0.82	93.13	93.59	84.84	73.95
14	0	14.22	47.77	694.73	0.81	93.57	94.52	82.50	72.96
16	0	12.93	49.15	756.15	0.79	93.90	95.30	78.13	69.91
7.8	50	15.89	221.50	626.10	1.11	73.87	87.50	61.59	39.81
10	50	15.61	222.74	686.09	1.10	75.49	90.13	68.74	46.77
12	50	14.66	224.65	746.90	1.06	76.88	91.90	70.00	49.45
14	50	13.13	226.20	808.30	1.00	78.13	93.32	66.32	48.36
16	50	11.31	228.90	865.62	0.93	79.09	94.52	60.19	45.00
7.8	100	15.92	205.32	619.97	1.14	75.12	87.30	62.46	40.96
10	100	15.67	206.90	680.28	1.11	76.68	89.99	69.67	48.07
12	100	14.76	208.80	742.37	1.08	78.05	91.77	71.03	50.87
14	100	13.43	210.56	804.93	1.02	79.27	93.20	68.21	50.39
16	100	11.80	212.18	864.33	0.94	80.29	94.45	62.96	47.75

Figure 11 shows the pump head H and efficiency η under five flow conditions. When R_a changed from $0 \mu\text{m}$ to $50 \mu\text{m}$, H and η were reduced, while the leakage amount q increased. When $Q = 7.8 \text{ m}^3/\text{h}$, the increase of R_a led to a decrease of H and η of 0.24 m and 22.6% , respectively, and q increased by $0.27 \text{ m}^3/\text{h}$. When $Q = 16 \text{ m}^3/\text{h}$, the increase of R_a led to a decrease of H and η of 1.62 m and 24.91% , respectively, and q increased by $0.14 \text{ m}^3/\text{h}$; When R_a increased from $50 \mu\text{m}$ to $100 \mu\text{m}$, H , η , and q increased together. When $Q = 7.8 \text{ m}^3/\text{h}$, with the increase of R_a , H , η , and q increased by 0.03 m , 1.15% , and $0.03 \text{ m}^3/\text{h}$, while they increased by 0.49 m , 2.75% , and $0.01 \text{ m}^3/\text{h}$ at $Q = 16 \text{ m}^3/\text{h}$. It showed that with the increase of flow rate, the influence of wall roughness on the head and efficiency increased gradually, but the influence on the leakage amount decreased gradually.

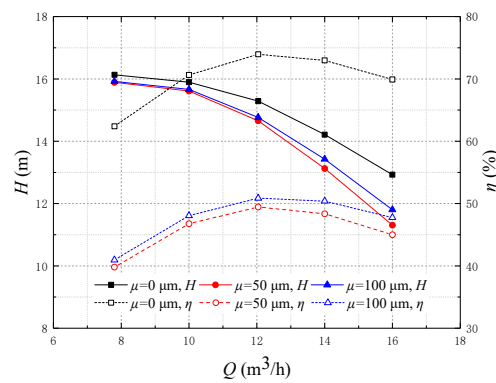


Figure 11. Pump’s performance with three kinds of wall roughness under different flow conditions.

Figure 12 shows the three kinds of power P_m , P_h , and P , with three kinds of wall roughness under five flow conditions. As Q increased, P_h and P showed an increasing trend, while P_m kept basically unchanged. With the increase of R_a , P_m , P_h , and P increased jointly, but the increasing rate kept the same with Q , indicating that the effect of wall roughness on the power was independent of Reynolds number.

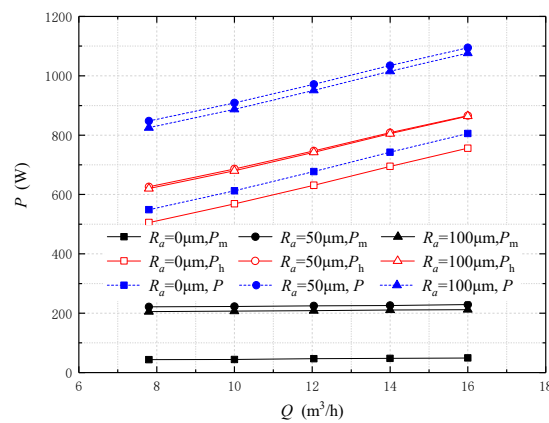


Figure 12. Three kinds of power of the pump under five flow conditions.

Figure 13 indicates the three kinds of efficiency η_m , η_h , and η_v under five flow conditions. With the increase of Q , η_m and η_v increased, while η_h first increased and then decreased. The reason why η_m increased was that P_m kept basically unchanged with the increase of Q , while P_h and P increased together, so the proportion of P_m in P gradually decreased. The reason why η_v increased was that the pump’s leakage amount decreased as with Q . The reason why η_h first increased and then decreased was that 12 m³/h was the design condition (optimal flow condition) of the pump. Under different roughness conditions, with the increase of flow rate, the variation amplitude of mechanical efficiency and volumetric efficiency decreased gradually, while the variation amplitude of hydraulic efficiency increased gradually. The reason why the variation amplitude of mechanical efficiency decreased gradually was that with the increase of flow rate, the variation amplitude of disk friction loss power and the roughness caused by disk friction loss power and hydraulic power basically remain unchanged, while the hydraulic power increased. The reason why the variation amplitude of volumetric efficiency decreased was that with increasing the flow rate, the influence of wall roughness on leakage also decreased gradually. When the roughness was less than the critical wall roughness, the reason for the increase of hydraulic efficiency was that with the increase of flow rate, the resistance loss along the pump path caused by roughness increased gradually. When the roughness was greater than the critical wall roughness, the reason for the increase of hydraulic efficiency was that with the increase

of roughness, the energy loss in the pump was close to a constant value [28], and the proportion decreased gradually.

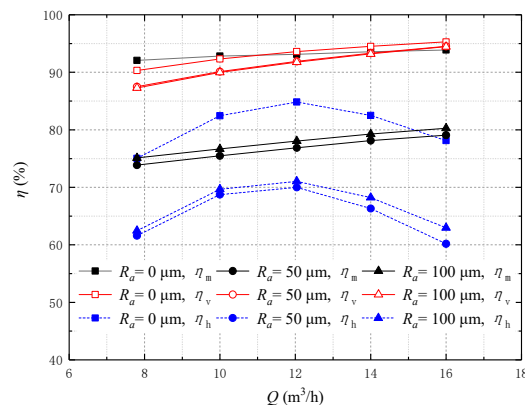


Figure 13. Three kinds of efficiency of the pump under five flow conditions.

4.5. Influence of Wall Roughness of Each Flow Part on the Pump Performance

To study the influence of wall roughness of each flow part on the pump performance, four flow parts of the pump, such as the impeller (including the blade and inner wall), shroud, pump cavity, and volute, were selected as research objects, and the wall roughness was set separately for numerical calculation. Figure 14 shows the pump head H with different wall roughness R_a of each flow part. It could be seen that with the increase of R_a of the impeller and shroud, the working capacity of the pump was improved, and H was gradually increased, but the increase rate was continuously decreased. The influence of R_a of the impeller on H was greater than that of the shroud. After considering the wall roughness of the pump cavity and volute, as R_a increased, H gradually decreased, and the decreasing rate continuously decreased. The influence of rough volute on the head was greater than that of all rough flow parts, indicating that the wall roughness of each flow part had no independent influence on the pump head, but interacted with each other.

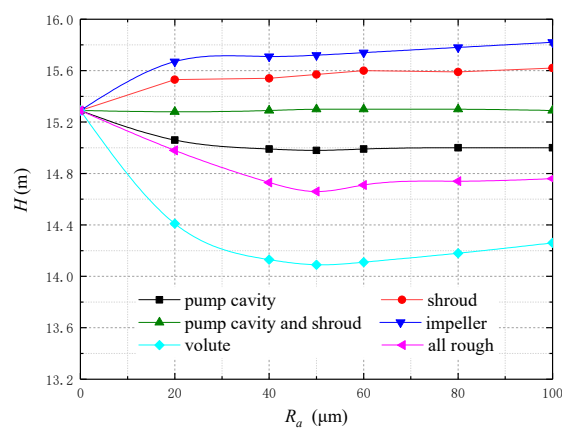


Figure 14. Pump's head with different wall roughness of each flow part under the rated flow condition.

Figure 15 shows the pump efficiency η with different wall roughness R_a of each flow part. It could be seen from Figure 15a that after considering the wall roughness of each flow part, η decreased with the increase of R_a , and the decreasing rate gradually reduced. When R_a reached the critical wall roughness ($R_a > 50 \mu\text{m}$), η kept stable basically. The influence of R_a of the impeller and shroud (pump cavity and volute) on η was basically the same, while the influence of R_a of the pump cavity and volute on η was greater than that of the impeller and shroud. The comprehensive influence of wall roughness of all the flow parts on the pump efficiency was smaller than the sum influence of that of

each flow part, indicating once again that the influence of wall roughness on the pump performance was interconnected. Figure 15b shows the mechanical efficiency η_m with different wall roughness R_a of each flow part. It could be seen that R_a of the impeller and volute had little effect on η_m , while that of the shroud and pump cavity had a strong effect on η_m . Obviously, R_a of the shroud was most sensitive to η_m of the pump, indicating that the disk friction loss was closely related to the wall roughness of the shroud. Figure 15c shows the volumetric efficiency η_v of the pump with different wall roughness R_a of each flow part. It could be seen that R_a of the impeller and shroud had a positive effect on η_m , while that of the volute and pump cavity had a negative effect. Moreover, R_a of the shroud and pump cavity was rather sensitive to η_v , indicating the flow in the pump cavity was closely related to the volumetric leakage. Figure 15d shows the hydraulic efficiency η_h of the pump with different wall roughness R_a of each flow part. It could be seen that R_a of the shroud had a slight positive effect on η_m , while that of the pump cavity, impeller, and volute had an obvious negative effect. The wall roughness of the volute was most sensitive to the hydraulic loss. In summary, the volumetric efficiency was affected by the wall roughness of the pump cavity and shroud, the mechanical efficiency was affected by the wall roughness of the shroud, and the hydraulic efficiency was affected by the wall roughness of the impeller and volute.

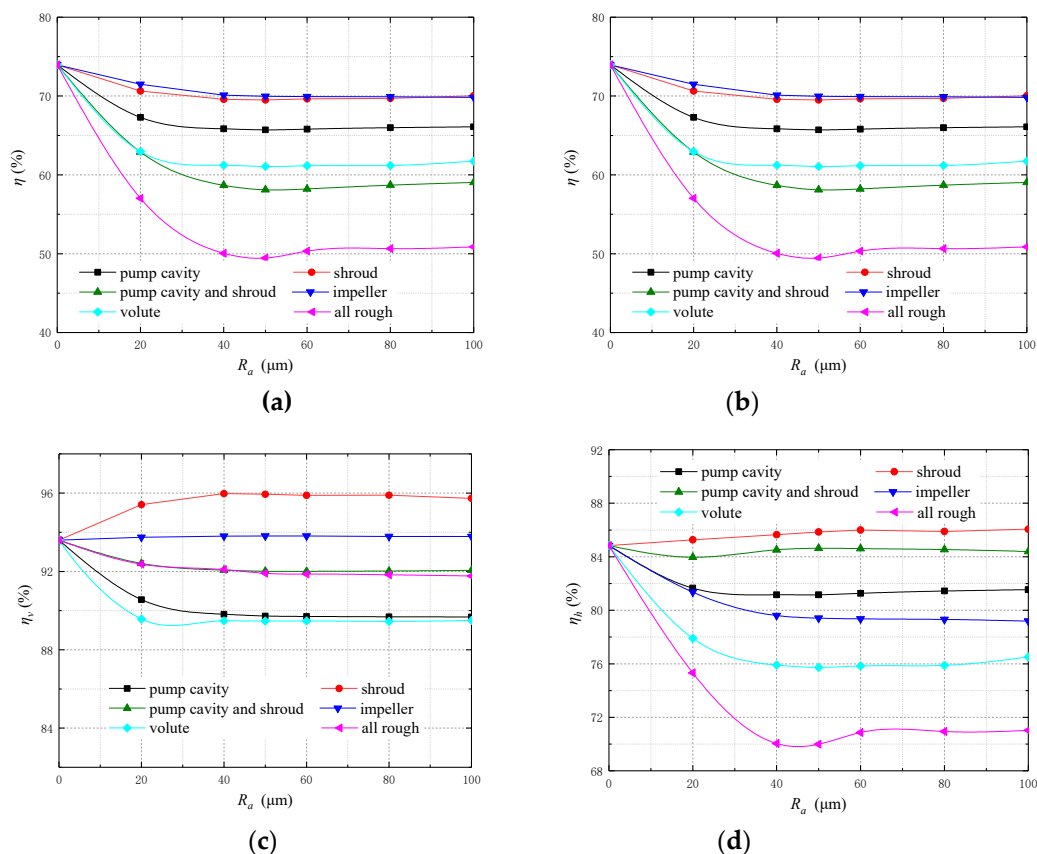


Figure 15. Pump efficiency η with different wall roughness R_a of each flow part under the rated flow condition: (a) total efficiency; (b) mechanical efficiency; (c) volumetric efficiency; (d) hydraulic efficiency.

Figure 16 shows the shaft power P with different wall roughness R_a of each flow part. As could be seen from Figure 16a, after considering the wall roughness of the volute, shroud, impeller, and pump cavity, respectively, P increased with the increase of R_a , and the increasing rate gradually reduced to zero when R_a reached to the critical value of the wall roughness. Figure 16b shows the disk friction loss power P_m . It could be seen that R_a of the impeller had little effect on P_m , while P_m increased with the R_a of the volute, pump cavity, and shroud. Obviously, R_a of the shroud had the most effects on the P_m of the pump. Figure 16c shows the hydraulic power P_h of the pump. It could be seen that R_a of the

shroud had a negative effect on P_h , while P_h increased with the R_a of the volute, pump cavity, and impeller. Obviously, R_a of the impeller had the most effects on P_h . In conclusion, the disk friction loss power was affected by the wall roughness of the shroud, while the hydraulic power was affected by that of the impeller.

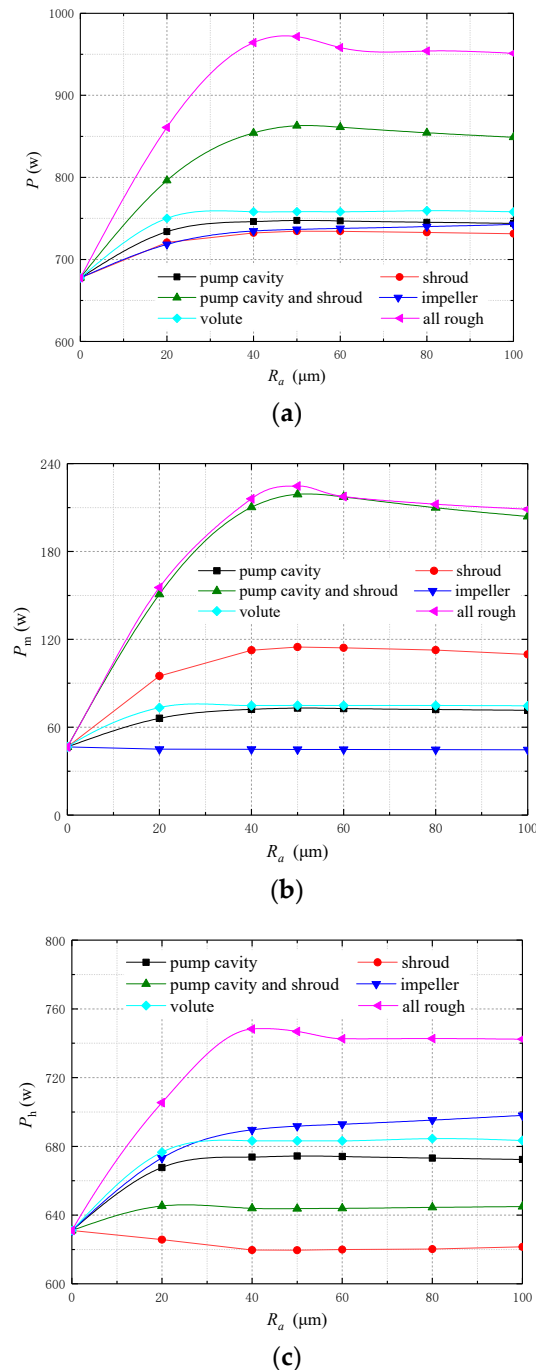


Figure 16. Shaft power P of the pump with different wall roughness R_a of each flow part: (a) total power; (b) disk friction loss power; (c) hydraulic power.

4.6. Comparison Between the Numerical and Experimental Results

The prototype of the pump was made, and the relevant experimental results could also be obtained. The whole experiment could be divided into four steps:

1. The original model was processed and then tested (All rough);

2. The impeller channel was polished and then tested (Smooth impeller channel);
3. The front and the rear shroud of the impeller were polished (Smooth shroud);
4. The volute channel and the inner wall of the pump cavity were polished (All smooth).

Every test was repeated to ensure the accuracy of the experimental data. After polishing the wall, the average wall roughness was about $5\ \mu\text{m}$. The schematic diagram of the test bench is shown in Figure 17. A turbine flowmeter was used to measure the flow Q , and the precision of the turbine flowmeter was $\pm 0.3\%$. Speed n was measured by a tachometer (PROVA RM-1500, Taiwan). During the experiment, only one dynamic pressure transmitters (CYG1401) was used to measure the outlet pressure. The precision of CYG1401 was $\pm 0.2\%$.

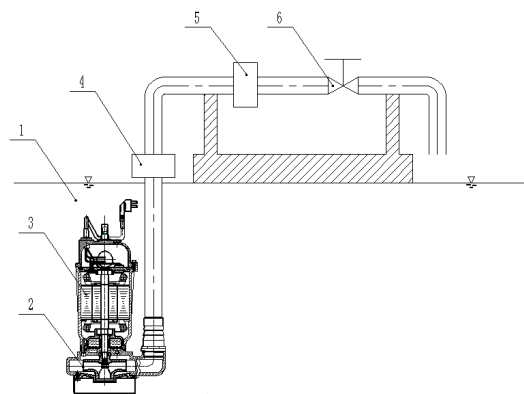


Figure 17. Schematic diagram of the test rig. 1. Pool; 2. Pump; 3. Motor; 4. Outlet pressure transmitters; 5. Turbine flowmeter; 6. Flow control valve.

Figure 18 illustrates the numerical and experimental results of the pump with four steps under five flow conditions ($Q = 7.8, 10, 12, 14, 16\ \text{m}^3/\text{h}$). As could be seen from Figure 18a, the experimental value of the head was consistent with the numerical value. When all the flow parts were smooth, the experimental and numerical head of the pump was largest. From Figure 18b, it could be seen that the numerical value of the efficiency was slightly higher than the experimental value because there is some backflow or deflow in the pump, and it's rather difficult to simulate the disordered flow by using CFD. Moreover, the numerical calculation did not consider the mechanical friction loss power at the bearing seal of the bearing shaft, which might account for 1% to 2% of the total power. However, the deviation between the numerical and experimental efficiency was only within 3%. Therefore, it's rather reliable to predict the pump's performance by using CFD.

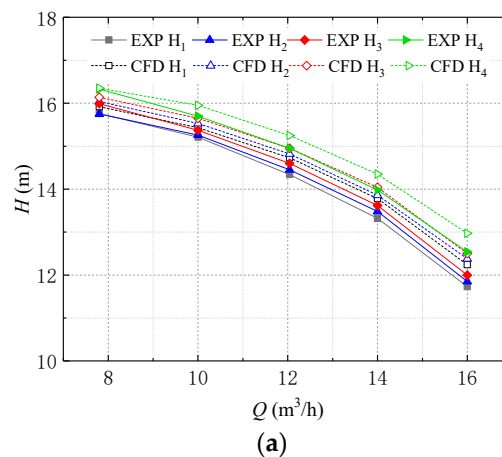


Figure 18. Cont.

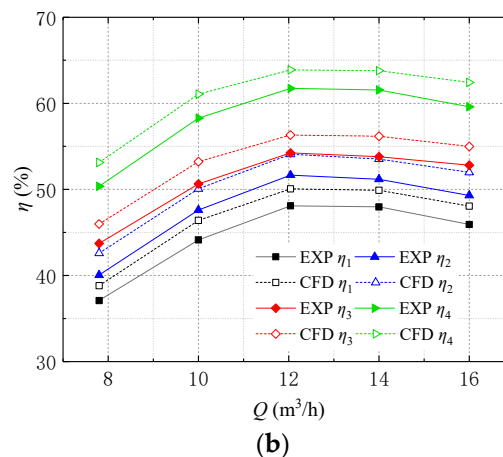


Figure 18. Numerical and experimental results of the pump with four steps under five flow conditions: (a) head; (b) efficiency.

5. Conclusions

- (1) Wall roughness affected the performance of the double-channel swage pump, and there was also a critical wall roughness. When the wall roughness was less than the critical wall roughness, the wall roughness had a great effect on the performance of the pump. With increasing the wall roughness, the efficiency and head were reduced, and the shaft power was increased. The effect of wall roughness on the shaft power and efficiency was much greater than that on the head. When the roughness exceeded the critical wall roughness, the wall roughness had little effect on the performance of the pump.
- (2) The volumetric efficiency was affected by the wall roughness of the pump cavity and shroud, the mechanical efficiency was affected by the wall roughness of the shroud, and the hydraulic efficiency was affected by the wall roughness of the impeller and volute. In addition, the effect of the wall roughness of different flow parts was interactive.
- (3) For general centrifugal pumps, reducing the volumetric leakage loss was the most effective way to increase pump efficiency. Moreover, it was beneficial to improving the pump efficiency and reducing the pump shaft power by polishing the shroud and pump cavity.
- (4) On the basis of the complete calculation model and appropriate numerical method, it was rather reliable to use CFD to predict the performance of the double-channel sewage pump.

Author Contributions: C.W. conceived and designed the experiments; Y.Z. and C.Z. performed the experiments and simulation; L.C. and K.C. analyzed the data; X.H. and B.H. wrote the paper; L.C. funding acquisition. All authors have read and agreed to the published version of the manuscript.

Funding: This work was supported by a project funded by the Priority Academic Program Development of Jiangsu Higher Education Institutions (PAPD), Nature Science Foundation of China (Grant No. 51609105 and No. 51979240).

Conflicts of Interest: The authors declare no conflicts of interest.

References

1. Wang, C.; He, X.; Shi, W.; Wang, X.; Wang, X.; Qiu, N. Numerical study on pressure fluctuation of a multistage centrifugal pump based on whole flow field. *AIP Adv.* **2019**, *9*, 035118. [[CrossRef](#)]
2. Chang, H.; Shi, W.; Li, W.; Wang, C.; Zhou, L.; Liu, J.; Yang, Y. Agarwal Rameshe. Experimental optimization of jet self-priming centrifugal pump based on orthogonal design and grey-correlational method. *J. Therm. Sci.* **2019**. [[CrossRef](#)]
3. Lu, Y.; Zhu, R.; Wang, X.; Wang, Y.; Fu, Q.; Ye, D. Study on the complete rotational characteristic of coolant pump in the gas-liquid two-phase operating condition. *Ann. Nucl. Energy* **2019**, *123*, 180–189.

4. Bai, L.; Zhou, L.; Jiang, X.; Pan, Q.; Ye, D. Vibration in a multistage centrifugal pump under varied conditions. *Shock Vib.* **2019**, *2019*, 2057031. [[CrossRef](#)]
5. Wang, C.; Hu, B.; Zhu, Y.; Wang, X.; Luo, C.; Cheng, L. Numerical study on the gas-water two-phase flow in the self-priming process of self-priming centrifugal pump. *Processes* **2019**, *7*, 330. [[CrossRef](#)]
6. Bhushan, S.; Ståhl, A.; Nilsson, S. Submersible wastewater pump association. *World Pumps* **2000**, *2000*, 44.
7. Chen, B.; Zhang, K.W. Characteristics and significance of high head submersible sewage pump for Three Gorges Project. *Pump Technol.* **2002**, *2002*, 23–25.
8. Zhao, B.; Hou, D.; Chen, H. Influence of impeller runner structure on performance of dual-channel pump. *J. Drain. Irrig. Mach. Eng.* **2013**, *31*, 294–299.
9. Minggao, T.; Rong, D.; Houlin, L.; Liang, D.; Naichang, H. Analysis on pressure pulsation under different impeller diameters in double channel sewage pump. *Trans. Chin. Soc. Agric. Eng.* **2015**, *31*, 53–59.
10. Tan, M.G.; Lian, Y.C.; Wu, X.F. Transient dynamics in a two-channel pump. *J. Drain. Irrig. Mach. Eng.* **2017**, *35*, 17–22.
11. Wang, C.; He, X.; Zhang, D.; Hu, B.; Shi, W. Numerical and experimental study of the self-priming process of a multistage self-priming centrifugal pump. *Int. J. Energy Res.* **2019**, *43*, 4074–4092. [[CrossRef](#)]
12. Wang, C.; Shi, W.; Wang, X.; Jiang, X.; Yang, Y.; Li, W.; Zhou, L. Optimal design of multistage centrifugal pump based on the combined energy loss model and computational fluid dynamics. *Appl. Energy* **2017**, *187*, 10–26. [[CrossRef](#)]
13. Hu, B.; Li, X.; Fu, Y.; Zhang, F.; Gu, C.; Ren, X.; Wang, C. Experimental investigation on the flow and flow-rotor heat transfer in a rotor-stator spinning disk reactor. *Appl. Therm. Eng.* **2019**, *162*, 114316. [[CrossRef](#)]
14. Wang, C.; Chen, X.X.; Qiu, N.; Zhu, Y.; Shi, W.D. Numerical and experimental study on the pressure fluctuation, vibration, and noise of multistage pump with radial diffuser. *J. Braz. Soc. Mech. Sci. Eng.* **2018**, *40*, 481. [[CrossRef](#)]
15. Li, X.; Chen, B.; Luo, X.; Zhu, Z. Effects of flow pattern on hydraulic performance and energy conversion characterisation in a centrifugal pump. *Renew. Energy* **2020**. [[CrossRef](#)]
16. Yang, H.; Zhang, W.; Zhu, Z. Unsteady mixed convection in a square enclosure with an inner cylinder rotating in a bi-directional and time-periodic mode. *Int. J. Heat Mass Transf.* **2019**, *136*, 563–580. [[CrossRef](#)]
17. Hemeida, A.M. Effect of wall roughness in turbulent pipe flow of a pseudoplastic crude oil: An evaluation of pipeline field data. *J. Pet. Sci. Eng.* **1993**, *10*, 163–170. [[CrossRef](#)]
18. Kandlikar, S.G. Roughness effects at microscale-reassessing Nikuradse's experiments on liquid flow in rough tubes. *Bull. Pol. Acad. Sci. Tech. Sci.* **2005**, *53*, 343–349.
19. Li, D.; Kang, Y.; Wang, X.; Ding, X.; Fang, Z. Effects of nozzle inner surface roughness on the cavitation erosion characteristics of high speed submerged jets. *Exp. Therm. Fluid Sci.* **2016**, *74*, 444–452. [[CrossRef](#)]
20. Tang, G.H.; Li, Z.; He, Y.L.; Tao, W.Q. Experimental study of compressibility, roughness and rarefaction influences on microchannel flow. *Int. J. Heat Mass Transf.* **2007**, *50*, 2282–2295. [[CrossRef](#)]
21. Gamrat, G.; Favre-Marinet, M.; Le Person, S.; Baviere, R.; Ayela, F. An experimental study and modelling of roughness effects on laminar flow in microchannels. *J. Fluid Mech.* **2008**, *594*, 399–423. [[CrossRef](#)]
22. Li, D.; Fan, Z.; Zhang, J.; Yang, X. Research on the impact of compressor blade roughness on its performance decline. *Aero Engine* **2009**, *5*, 36–39.
23. Li, F.; Bu, Q. Effect of relative roughness of flow path of similar fans on its flow efficiency. *FAN Technol.* **2009**, *1*, 31–32.
24. Li, C.; Liang, Q.; Zhao, Y. Effect of surface roughness on micro-gap leakage of oil-free scroll compressors. *Fluid Mach.* **2011**, *4*, 47–50.
25. Gao, L. Experimental Research on the Effect of Surface Roughness on the Performance of Compressor Cascades. Ph.D. Thesis, University of Chinese Academy of Sciences, Beijing, China, 2015.
26. Han, F.; Du, L.; Li, W.; Li, C. Effect of blade surface roughness on the aerodynamic performance of compressors in a class environment. *J. Dalian Jiaotong Univ.* **2015**, *2*, 50–54.
27. Wang, C.; He, X.; Cheng, L.; Luo, C.; Xu, J.; Chen, K.; Jiao, W. Numerical Simulation on Hydraulic Characteristics of Nozzle in Waterjet Propulsion System. *Processes* **2019**, *7*, 915. [[CrossRef](#)]
28. Jiao, W.; Cheng, L.; Zhang, D.; Zhang, B.; Su, Y.; Wang, C. Optimal design of inlet passage for waterjet propulsion system based on flow and geometric parameters. *Adv. Mater. Sci. Eng.* **2019**, *2019*, 2320981. [[CrossRef](#)]

29. Zhu, Y.; Tang, S.; Wang, C.; Jiang, W.; Yuan, X.; Lei, Y. Bifurcation Characteristic research on the load vertical vibration of a hydraulic automatic gauge control system. *Processes* **2019**, *7*, 718. [[CrossRef](#)]
30. Zhu, Y.; Tang, S.; Wang, C.; Jiang, W.; Zhao, J.; Li, G. Absolute stability condition derivation for position closed-loop system in hydraulic automatic gauge control. *Processes* **2019**, *7*, 766. [[CrossRef](#)]
31. Zhu, Y.; Tang, S.; Quan, L.; Jiang, W.; Zhou, L. Extraction method for signal effective component based on extreme-point symmetric mode decomposition and Kullback-Leibler divergence. *J. Braz. Soc. Mech. Sci. Eng.* **2019**, *41*, 100. [[CrossRef](#)]
32. Zhu, Y.; Qian, P.; Tang, S.; Jiang, W.; Li, W.; Zhao, J. Amplitude-frequency characteristics analysis for vertical vibration of hydraulic AGC system under nonlinear action. *AIP Adv.* **2019**, *9*, 035019. [[CrossRef](#)]
33. He, X.; Jiao, W.; Wang, C.; Cao, W. Influence of surface roughness on the pump performance based on Computational Fluid Dynamics. *IEEE Access* **2019**, *7*, 105331–105341. [[CrossRef](#)]
34. Guelich, J.F. Effect of Reynolds Number and Surface Roughness on the Efficiency of Centrifugal Pumps. *J. Fluids Eng.* **2003**, *125*, 670–679. [[CrossRef](#)]
35. Zhu, H.; Zhai, B.; Zhou, J. Study on the Influence of Wall Roughness on Hydraulic Performance of Axial Flow Pump. *J. Irrig. Drain.* **2006**, *25*, 87–90.
36. Yamazaki, Y.; Nakayama, T.; Narabayashi, T.; Kobayashi, H.; Shakouchi, T. Effect of Surface Roughness on Jet Pump Performance. *JSME Int. J. Ser. B* **2006**, *49*, 928–932. [[CrossRef](#)]
37. Aldas, K.; Yapici, R. Investigation of Effects of Scale and Surface Roughness on Efficiency of Water Jet Pumps Using CFD. *Eng. Appl. Comput. Fluid Mech.* **2014**, *8*, 14–25. [[CrossRef](#)]
38. Feng, J.J.; Zhu, G.J.; He, R. Effect of surface roughness on the performance of axial flow pump. *J. Northwest Univ. Nat. Sci. Ed.* **2016**, 196–202.
39. Pan, Z.Y.; Gu, L.Q.; Gu, M.F. Numerical simulation analysis of flow field characteristics of axial flow pump with wall roughness. *Water Technol. Econ.* **2018**, *24*, 43–46.
40. Deshmukh, D.; Siddique, M.H.; Kenyery, F.; Samad, A. Critical surface roughness for wall bounded flow of viscous fluids in an electric submersible pump. In Proceedings of the APS Meeting Abstracts, New Orleans, LA, USA, 13–17 March 2017.
41. Gu, M.F.; Yang, X.H.; Sun, F.M. Study on the influence of different roughness on the hydraulic performance of axial flow pump. *Tech. Superv. Water Resour.* **2018**, *6*, 146–148.
42. Lim, S.E.; Sohn, C.H. CFD analysis of performance change in accordance with inner surface roughness of a double-entry centrifugal pump. *J. Mech. Sci. Technol.* **2018**, *32*, 697–702. [[CrossRef](#)]
43. CFX-Solver Theory Guide, ANSYS 13.0 Help [EB/OL]. 2010. Available online: <http://www.doc88.com/p-908539666887.html> (accessed on 6 October 2012).
44. Brian Whalley, W.; Rea, B.R. A digital surface roughness meter. *Earth Surf. Processes Landf.* **1994**, *19*, 809–814. [[CrossRef](#)]
45. Johnson, F.; Brisco, B.; Brown, R.J. Evaluation of limits to the performance of the surface roughness meter. *Can. J. Remote Sens.* **1993**, *19*, 140–145. [[CrossRef](#)]
46. Yan, Z.; Yong, T. Uncertainty Analysis and Calculation of Surface Roughness Comparison Sample Measurement. *Mod. Meas. Lab. Manag.* **2009**, *4*, 30–31.
47. Zhao, B.; Wang, Y.; Chen, H. Impact of wall roughness on the flow law in chamber of a centrifugal pump at off-design operating condition. *J. Eng. Thermophys.* **2015**, *36*, 1927–1932.
48. Sun, H.; Ye, N.; Wang, S. Effect of Roughness on Boundary Layer Flow and Aerodynamic Performance of Compressor. *J. Harbin Eng. Univ.* **2017**, *38*, 554–560.
49. Colebrook, C.F.; White, C.M. Experiments with fluid friction in roughened pipes. *Proc. R. Soc. Lond. Ser. A Math. Phys. Sci.* **1937**, *161*, 367–381.
50. Adams, T.; Grant, C.; Watson, H. A simple algorithm to relate measured surface roughness to equivalent sand-grain roughness. *Int. J. Mech. Eng. Mechatron.* **2012**, *1*, 66–71. [[CrossRef](#)]
51. Deshmukh, D.; Samad, A. CFD-based analysis for finding critical wall roughness on centrifugal pump at design and off-design conditions. *J. Braz. Soc. Mech. Sci. Eng.* **2019**, *41*, 58. [[CrossRef](#)]

